# Efficient, Nonintrusive Outcoupling in Organic Light Emitting Devices Using Embedded Microlens Arrays

Yue Qu,[†] Jongchan Kim,[†] Caleb Coburn,[‡] and Stephen R. Forrest[*,†,‡,§]

[†]Department of Electrical Engineering and Computer Science, University of Michigan, Ann Arbor, Michigan 48109, United States
[‡]Department of Physics, University of Michigan, Ann Arbor, Michigan 48109, United States
[§]Department of Materials Science and Engineering, University of Michigan, Ann Arbor, Michigan 48109, United States

ABSTRACT: We demonstrate efficient light extraction from the active region of bottom-emitting organic light emitting devices (OLEDs) using a high refractive index, nondiffractive hemispherical microlens array located between the transparent anode and embedded in the low refractive index glass substrate ($n = 1.5$). The subelectrode microlens array (SEMLA) results in a maximum external quantum efficiency of $70 \pm 4\%$ for green phosphorescent OLEDs (PHOLEDs). Furthermore, the wavelength- and viewing-angle-independent light extraction structure results in white PHOLED external efficiencies of $50 \pm 3\%$. The SEMLA light extraction structure is nonintrusive; that is, it lies completely outside of the OLED structure. Since this design has no effect on the image resolution, it is compatible with applications for both displays and white light illumination, with no dependence on molecular transition dipole orientation and the active organic layers (and hence diode electrical characteristics) used in the PHOLED. Finally, due to the micrometer-scale feature size of the SEMLA, it is achieved using conventional photolithography prior to the OLED array deposition.

KEYWORDS: light extraction, white OLED, multimicrometer scale, high refractive index, phosphorescent OLED
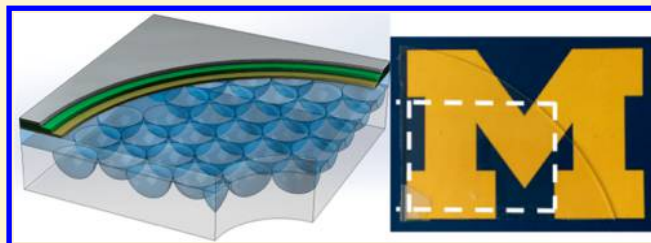
Numerous challenges toward commercialization of organic light emitting devices (OLEDs) have been overcome by the introduction of efficient phosphorescent OLEDs (PHO-LEDs),[1−3] doped transport layers,[4] and outcoupling schemes that have led to the OLED display revolution. However, while PHOLED internal quantum efficiencies (η_{IQE}) can reach 100%, most of the emission remains trapped without light extraction structures, resulting in external quantum efficiencie (η_{EQE}) of ∼20%.[5,6] The trapped light, due to the refractive index differences between the several layers in the structure, can be separated into three modes: substrate, waveguide, and surface plasmons. The substrate modes are trapped by total internal reflection at the glass—air interface. Substrate modes are conveniently extracted by microlens arrays (MLAs)[7] or scattering layers.[8] Waveguide modes trapped in the device active region result from the higher refractive indices, n, of organic layers and the indium tin oxide (ITO) anode ($n_{org} \approx 1.8$, $n_{ITO} = 1.9-2.1$) than the glass substrate ($n_{glass} = 1.45-1.5$). The surface plasmon mode is excited by emission in the near field and propagates along the metal—organic interface. Many techniques have been proposed to extract light from waveguide and surface plasmon modes, such as molecular transition dipole alignment,[9,10] specialized cavity designs,[11,12] photonic crystals,[13] high refractive index substrates,[14] scattering structures,[8,15,16] and so on.[8,17−20] Many methods are incompatible with existing organic materials or active region structures, producing undesired angular emission profiles, distortion of the emission spectra, or complicated and high-cost fabrication procedures. Recently, a high refractive index layer with sub-

micrometer-scale voids[21] beneath the transparent electrode has been shown to extract all optical power but surface plasmon modes, which is comparable to the performance of subanode air grids.[17] With an optimized white OLED active region, this method reached $\eta_{EQE} = 78\%$ with color stability across all viewing angles. However, the fabrication procedure is complicated with potentially high costs.

Here we demonstrate a simple, efficient, and wavelength-independent method for extracting trapped light in the active region into the air and substrate modes by embedding a microlens array between a transparent electrode and the glass substrate. The subelectrode microlens array (SEMLA) shown in Figure 1a consists of a flat spacer layer on top of a hexagonal closed-packed array of 10 μm diameter hemispherical lenses with a refractive index (n_{SEMLA}) of 1.8. The microlens trenches in the glass substrates show the hemispherical shape of the SEMLA in Figure 1b. The lenses are closely packed, leaving no flat plateau area in between. The SEMLA surface is smooth, eliminating optical scattering from the structure. The dimension is based on the previous studies,[7] with no further optimization. The structure does not intrude into the device active region and, hence, places no constraints on the design of the OLED itself. The lens array is fabricated using conventional photolithography (see Methods) while being much smaller than a display pixel size (typically >30 μm). Figure 1b shows a glass substrate containing the SEMLA structure (highlighted by
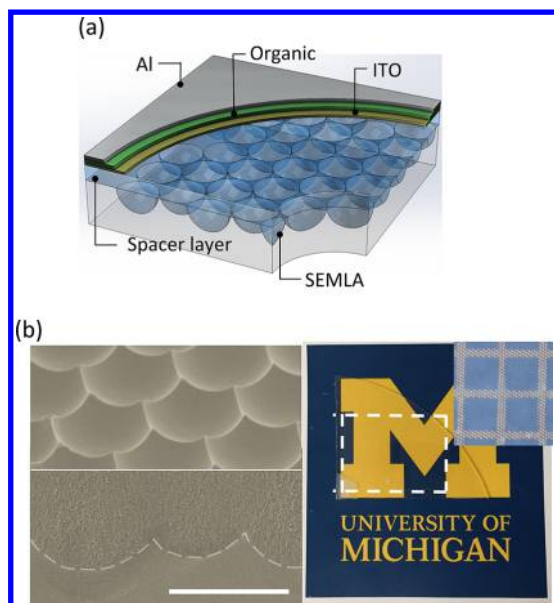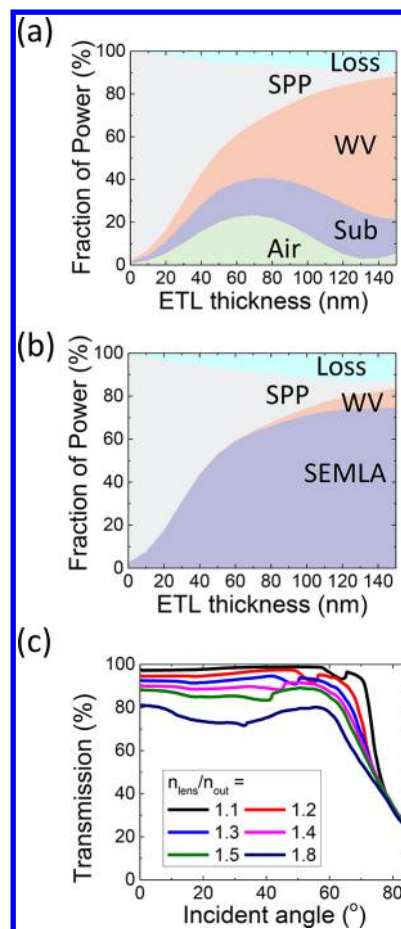
Figure 1. (a) Schematic illustration of devices on a subelectrode microlens array (SEMLA) substrate. (b) Left: Scanning electron microscope image of the microlens-shaped trenches in glass substrates (upper) and the cross section of a SEMLA substrate with a dashed line highlighting the interface between the lenses and the glass (bottom). Right: Image of a SEMLA substrate on a printed image, with the microlens side facing the image. The white dashed lines enclose the SEMLA structure area. Inset: Microscopic image of a SEMLA on top of a substrate patterned with a square grid with a 100 μm pitch and 20 μm wide gridlines. Use of the logo is by permission.


Figure 2. Optical power modal analysis vs electron transport layer (ETL) thickness on (a) a conventional glass substrate and (b) a SEMLA substrate. The power is distributed into air, substrate (Sub), waveguide (WV), surface plasmon polariton (SPP) and lossy metal (Loss) modes. (c) Ray tracing simulation results for the transmission through a microlens (n_{lens}) to the medium in which it is embedded (n_{out}) vs incident angle to substrate normal.

dashed lines) on a printed background, with no apparent impact on the image sharpness. Figure 1b, inset, shows a microscopic image of a section of a glass substrate covered by the SEMLA structure. The substrate is patterned with a square grid with a 100 μm period and 20 μm wide metal gridlines, which is comparable to a mobile phone display pixel size. The SEMLA has a negligible impact on image resolution when magnified at this level.

The high refractive index of the SEMLA extracts waveguide modes from organic and ITO anode layers. Figure 2a and b show the calculated optical power distribution in the devices with and without the SEMLA based on Green's function analysis, assuming that the spacer layer is semi-infinite (see Methods). The device structure used in the calculation is the following: 40 nm ITO anode/40 nm hole transport layer/20 nm emission layer/electron transport layer/Al cathode. For the SEMLA refractive index of $n_{SEMLA} = 1.8$, the waveguide modes are reduced to almost zero for an electron transport layer thickness of <70 nm, with the SEMLA structure extracting all radiated optical power except for the surface plasmon modes. The optical power exits into the glass substrate from the high-index hemispherical microlens array. The light extraction from the SEMLA into glass ($n_{glass} = 1.45$) is more efficient than from an external MLA ($n_{MLA} = 1.4-1.5$) into air ($n_{air} = 1$) due to reduced reflection at the lens/glass interface with its larger critical angle. This behavior has been verified by a ray tracing simulation (see Methods), with results in Figure 2c. The discontinuities in the transmission spectra result from total internal reflection at the flat plateaus between the lenses. As the ratio of refractive indices of the microlens (n_{lens}) to the medium in which it is embedded (n_{out}) increases, the transmission at all incident angles decreases. Thus, n_{SEMLA} is chosen to be high

enough to suppress waveguide modes in the organic and ITO layers, but not so high that the array itself becomes waveguiding. Air gaps between the substrate and the MLA, as demonstrated previously,[22] increase reflections and, hence, should be avoided. Since the total transmission through a microlens array also depends on the angular profile of the emission source, the light extraction efficiency into the substrate may vary for different organic cavities.

To demonstrate the enhancement in light extraction, green and white PHOLEDs (WOLEDs) were fabricated on conventional glass, sapphire ($n_{sapphire} = 1.77$), and SEMLA substrates. An external MLA was also attached to SEMLA substrates to further enhance outcoupling. The total quantum efficiency of both air and substrate modes was measured using a commercial index matching fluid (IMF) to measure the extraction efficiency of trapped light from the ITO and organic layers. The IMF indices were $n_{IMF,low} = 1.51$ for the SEMLA and conventional glass substrates and $n_{IMF,high} = 1.70$ for sapphire, enabling outcoupling of substrate modes.

The performance characteristics of the green PHOLEDs with different substrates are shown in Figure 3. All devices have identical electrical characteristics since the SEMLA does not intrude into the device active region. The green-emitting device
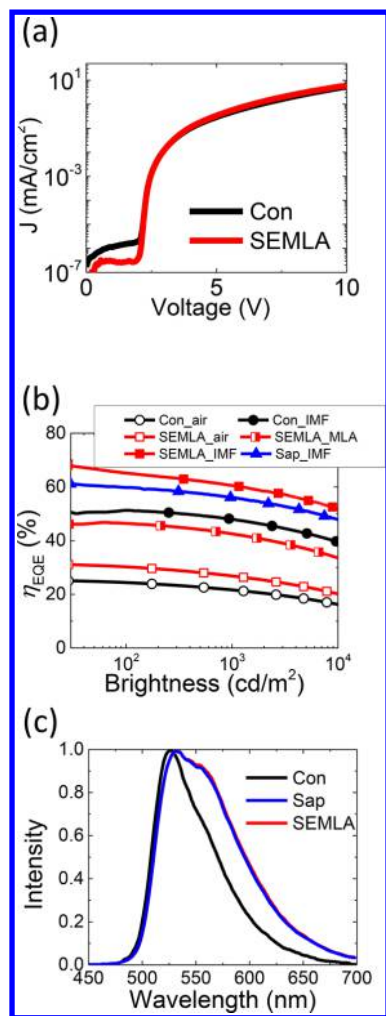
Figure 3. Measured characteristics of green phosphorescent organic devices (PHOLEDs) on conventional flat glass (Con), SEMLA, and sapphire (Sap) substrates. Measurements with no additional outcoupling at the substrate and air interface (air), with an external microlens array (MLA), and with index matching fluid (IMF) are indicated. (a) Current density (J)−voltage characteristics of the SEMLA and conventional devices showing no significant differences. (b) External quantum efficiencies (η_{EQE}) of PHOLEDs on different substrates. (c) Spectra of green PHOLEDs on different substrates with no additional outcoupling at the substrate/air interface.

comparisons are obtained at a luminance of 100 cd/m^2. The SEMLA alone enhances η_{EQE} from 25 ± 3% for a PHOLED on a flat glass substrate to 30 ± 3%, representing an improvement by an outcoupling enhancement factor (EF) of 1.2. The outcoupling is further enhanced by EF = 1.9 to η_{EQE} = 47 ± 4% using an external MLA to improve substrate outcoupling. Using IMF at the glass−air interface in conjunction with the SEMLA extracts 65 ± 5% (an EF = 2.6) of the total generated photons, compared with 51 ± 4% for conventional glass and 60 ± 4% for sapphire substrates. The most efficient device using the SEMLA reaches η_{EQE} = 70 ± 4%. The spectra of PHOLEDs employing the SEMLA along with sapphire substrates are identical. It is slightly broader than that from conventional glass substrates due to weaker cavity effects in the SEMLA since $n_{SEMLA} \approx n_{sapphire} \approx n_{org}$.

The optical output characteristics of white PHOLEDs (WOLEDs) are shown in Figure 4. The SEMLA enhances η_{EQE} from 16 ± 2% for conventional glass substrates to 20 ±

2% by EF = 1.3. It can be further enhanced to 27 ± 3% using an external MLA with EF = 1.7. Using an IMF, the SEMLA extracts 45 ± 4% (EF = 2.8) of the total generated photons into the glass substrate, compared with 37 ± 3% for conventional glass and 41 ± 3% for sapphire substrates. The most efficient WOLED using the SEMLA reaches η_{EQE} = 50 ± 3% by EF = 3.1. This is one of the most efficient WOLEDs reported,[22−24] limited primarily by the efficiency of the device[25] rather than the outcoupling scheme. The spectra from the three different substrates without an external MLA are shown in Figure 4b. Both sapphire and SEMLA substrates have high intensities in the red and blue spectral regimes compared with the conventional glass substrate, showing boarder spectra resulting from weaker cavity effects.

The WOLED spectra at different viewing angles on a glass, a SEMLA substrate with an external MLA (SEMLA MLA), and a SEMLA substrate with a large hemispherical outcoupling lens (SEMLA HS) are shown in Figure 4c. The spectral blue shift at large angles is only observed for the control device. The SEMLA eliminates this common spectral shift at large angles, making it more suitable for display and white light illumination applications. The angular intensity profile of the conventional device is much narrower than a Lambertian source. In contrast, the SEMLA-modified substrates show higher intensities at large viewing angles, bringing them closer to a Lambertian source.

The simulated light extraction efficiency into the SEMLA (60% in Figure 2b) is lower than measurements (65 ± 5% in Figure 3b), even when assuming 100% transmission (Figure 2c) from the SEMLA into the glass substrate. The mismatch partially results from birefringence[26] (with ordinary and extraordinary indicies of refraction of n_o = 1.8 and n_e = 1.6, respectively) of the electron transporting layer comprising 4,6-bis(3,5-di-3-pyridylphenyl)-2-methylpyrimidine;4,6-bis(3,5-di-(pyridin-3-yl)phenyl)-2-methylpyrimidine (B3PYMPM), which is not considered in the simulation. The 10 to 30 μm thickness of the flat spacer layer is comparable with the coherence length of OLEDs,[27] but it is nevertheless treated in the simulation as a semi-infinite plane, which may be another source of the differences with measurement.

The SEMLA extracts more light than the direct fabrication of the WOLEDs on high-index sapphire substrates (Figure 3b and Figure 4a), despite the fact that $n_{sapphire} \approx n_{SEMLA}$ and there is less than 100% transmission from the SEMLA into glass. The lower efficiency of the sapphire substrate results from two sources. First, there is a minor refractive index mismatch between sapphire and the IMF ($n_{sapphire}$ = 1.77, $n_{IMF,high}$ = 1.70) that reduces the outcoupling of light trapped in the substrate. Second, since the SEMLA thickness is comparable to the WOLED coherence length, the optical power distribution in the SEMLA may be subject to destructive interference. The mismatches between measurement and simulation and between the devices on sapphire and SEMLA substrates show that the SEMLA has reached the theoretical limit for light extraction. This indicates that the SEMLA extracts all emitted optical power with the exception of residual surface plasmon modes. The surface plasmon modes can be further enhanced using a thick ETL, as shown in Figure 2b. Other SPP reduction strategies such as corrugated structures and optical gratings may also be integrated with the SEMLA, although they can potentially increase the fabrication complexity and costs.

The similar enhancement factors of light extraction from both the green and white PHOLEDs in Figure 5 indicate that the SEMLA solution is independent of emission wavelength, as
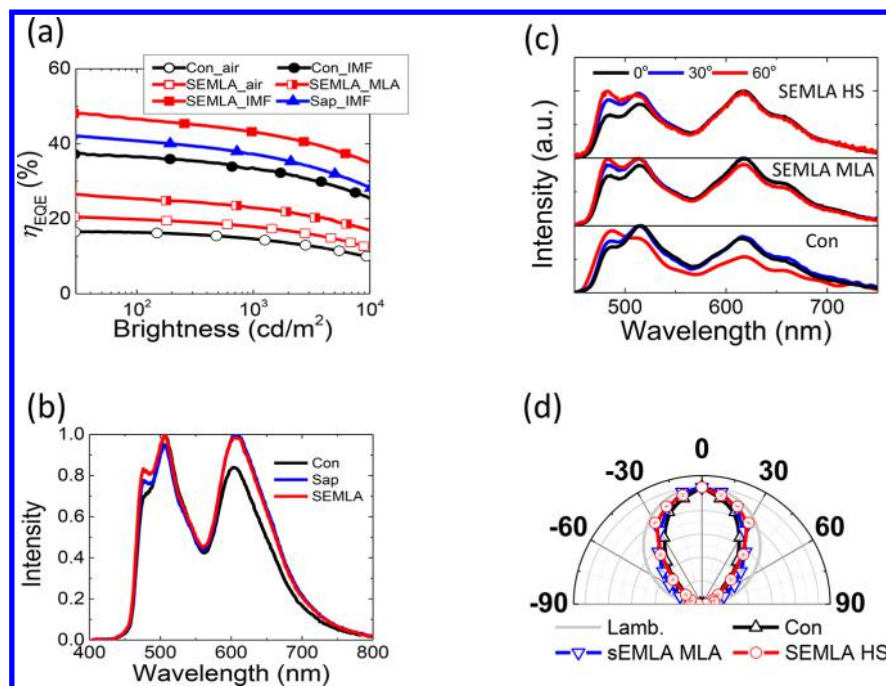
Figure 4. Measured characteristics of WOLEDs on conventional glass (Con), SEMLA, and sapphire (Sap) substrates. Measurements with no additional outcoupling at the substrate/air interface (air), with an external microlens array (MLA), and with index matching fluid (IMF) are indicated. (a) External quantum efficiency (η_{EQE}) of WOLEDs on different substrates. (b) WOLED spectra on different substrates. The spectra are collected at the same current density (J), at which the luminance of the control (L_{Con}) is 10 000 cd/m^2. (c) Spectra of devices on a conventional glass substrate (Con), a SEMLA substrate with an external MLA (SEMLA MLA), and a SEMLA substrate with a large hemispherical outcoupling lens with IMF (SEMLA HS) at 0°, 30°, and 60° to the substrate normal. The spectra were collected at the same J, at which L_{Con} = 5000 cd/m^2. (d) Angular luminosity distribution of WOLEDs on different substrates. Lamb. indicates an ideal Lambertian emission pattern.
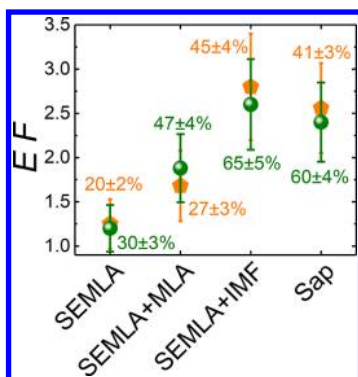
Figure 5. Enhancement factor (EF) of green and white PHOLEDs on different substrates shown in previous figures, compared with conventional flat substrates with identical OLED device structures. The η_{EQE} are indicated. The green circles and the orange pentagons denote the green and white PHOLEDS, respectively.

expected. The spectra on the SEMLA and sapphire substrates are almost identical since the structure is nondiffractive. This also provides a guideline for cavity designs of OLEDs on SEMLA substrates. Compared with high refractive index substrates, the glass–air interface of the SEMLA substrate can more readily outcouple substrate modes. When employing external MLAs, the outcoupling into air for n_{lens}/n_{out} = 1.5 is higher than for n_{lens}/n_{out} = 1.8 in Figure 2c. Thus, the SEMLA substrates replace sapphire substrates with higher efficiency and lower costs, at no expense to performance or freedom in device design.

An external MLA can enhance the η_{EQE}, but is not as efficient as the large hemispherical lens or the IMF, as shown in Figures

3b and 4a. The MLA only outcouples ~70% photons from the substrate and air modes combined. Figures 3b and 5 show that ~20% of photons remain trapped in the substrate using the SEMLA in combination with the MLA. Other technologies for substrate mode extraction[8] appear to exhibit the same bottleneck. Solutions to improve extraction from substrate modes are, therefore, necessary to fully exploit the advantages of efficient waveguide and surface plasmon mode outcoupling structures such as the SEMLA.

In summary, high refractive index subelectrode microlens arrays embedded in the glass substrate and beneath the transparent bottom electrode in OLEDs can redirect 100% of the light confined in organic and ITO layers toward the substrate. Its placement below the OLED allows complete freedom in OLED design and fabrication; the nonintrusive flat upper surface of the lens array provides a surface similar to that of a conventional flat glass or plastic substrate. Both monochromatic and white PHOLEDs fabricated on SEMLA substrates with external outcoupling show extremely high efficiencies of η_{EQE} = 70 ± 4% with EF = 2.8 for green and η_{EQE} = 50 ± 3% with EF = 3.1 for the WOLED compared to analogous devices on conventional glass substrates. This is significantly more efficient light extraction than other reports of nonintrusive outcoupling structures. The blue shift eliminated at large angles along with no perceptible impact on image sharpness makes this method ideal for white light illumination and display applications. The spectrum of WOLEDs on SEMLA substrates remains identical with those on sapphire substrates, affording both higher efficiency and lower costs with no expense to performance or freedom in device design.

METHODS

Optical Modal Analysis. Optical analysis assumes that an emitting dipole (wavelength of 540 nm) is located in the center of the emissive layer with a thickness of 20 nm and refractive index of 1.83. The emitting dipole has 77% horizontal and 23% vertical component emission due to dipole alignment of the green dopant material bis[2-(2-pyridinyl-N)phenyl-C](2,4-pentanedionato-$O2,O4$)iridium(III) (Ir(ppy)$_2$acac). The thicknesses and refractive indices of each layer are 40 nm thick ITO with n = 2.1, 40 nm thick hole transport layer with n = 1.70, emissive and electron transport layers with n = 1.78, and Al with a complex index of n = 0.6 + 2.8i. The SEMLA and polymer planarization layers (both made of NOA 170, Norland Products Inc.) have n = 1.8. All indices of refraction were measured with an ellipsometer. The glass refractive index is n = 1.45.

Ray Tracing Simulations. The geometry in the simulation was a hexagonal array of close-packed hemispherical microlenses with an ITO, an organic layer, and a reflective metal on its planar surface. The refractive indices of the ITO and organic materials are identical to that of the microlenses, so no refraction was considered between the microlens–substrate interface and the metal surface. A 3% loss per pass through the ITO and 8% loss per reflection at the metal surface were assumed. The light was assumed to be unpolarized. At each incidence angle, the transmission was calculated for >1000 rays evenly distributed over a unit cell and originating from within the organic layer. The azimuthal dependence was averaged to provide the transmission as a function of polar angle. To improve the computation speed, rays with a remaining relative intensity of <0.5% were eliminated.

Device Fabrication and Measurements. A photoresist (PR) layer spun onto a solvent-cleaned soda lime glass (UniversityWafer #3004169267) substrate was patterned with an I-line ×5 reduction AutoStep exposure system (GCA AS200) into a hexagonal array with 0.8 μm diameter circular openings with a 10 μm pitch. After a 10 min hard bake, the glass with patterned PR was immersed for 6.5 min in buffered HF Improved (Transene) diluted 6:1 with a surfactant. The PR was then removed by sonication in acetone and 2-proponal and a 20 min RCA cleaning step. The NOA-170 was spin-coated onto the etched glass substrate and cured under ultraviolet illumination. NOA-170 filled the etched microlens-shaped trenches and formed a ~20 μm thick flat layer above the microlens. After the subelectrode MLA preparation, a 40 nm thick ITO layer was deposited by radio frequency magnetron sputtering at 20 W in a chamber with an Ar pressure of 5 mTorr at a rate of 0.1 Å. The glass and sapphire substrates were cleaned by sonication in tergitol, deionized water, acetone, and 2-propanol and coated with ITO along with SEMLA substrates.

Organic layers and top electrodes were deposited by vacuum thermal evaporation in a system with a base pressure of 10^{-7} Torr. The green PHOLED consists of a 2 nm thick MoO$_3$, 40 nm thick 4,4′-cyclohexylidenebis[N,N-bis(4-methylphenyl)-benzenamine] (TAPC), 25 nm thick, 8 vol % Ir(ppy)$_2$acac doped in 4,4′-bis(carbazol-9-yl)biphenyl (CBP), and 65 nm B3PYMPM. The white PHOLED structure consists of 2 nm thick MoO$_3$, 50 nm thick TAPC, 15 nm thick 4 vol % Ir(ppy)$_2$acac, 4 vol % bis(2-methyldibenzo[f,h]quinoxaline)-(acetylacetonate)iridium(III) (Ir(MDQ)$_2$acac) co-doped in CBP, 10 nm thick bis[2-(4,6-difluorophenyl)pyridinato-$C2,N$]-(picolinato)iridium(III) (FIrpic) 10 vol % doped with CBP,

and 55 nm thick 3,3′,5,5′-tetra[(M-pyridyl)phen-3-yl]biphenyl (BP4MPy). Finally, the cathode consisting of 1.5 nm thick lithium quinolate and 100 nm thick Al was deposited through an array of 1 mm diameter openings in a shadow mask.

The refractive indices and thicknesses of materials were measured using a variable-angle spectroscopic ellipsometer (J. A. Woollam, WVASE32). To measure the refractive index of NOA 170, it was mixed with propylene glycol methyl ether acetate, spin-coated on a silicon substrate, baked, and annealed under an ultraviolet lamp. Current−voltage−luminance characteristics were collected using a semiconductor parameter analyzer (HP-4156A) and a calibrated Si photodiode. The electroluminescence spectra were measured using an Ocean Optics miniature spectrometer. The η_{EQE} was calculated using standard methods.[28] The systematic error in the measurement setup is 6%. The external microlens array (Lumlight, MA1303001) was applied at the glass substrate before measurements. To measure the total light intensity in both the air and substrate modes, index-matching fluid was applied between the substrates and the photodiode.

AUTHOR INFORMATION

Corresponding Author

*E-mail: stevefor@umich.edu.

ORCID ⓘ

Stephen R. Forrest: 0000-0003-0131-1903

Author Contributions

Y.Q. performed experiments, measurements, and modal analysis simulations. Y.Q. and J.K. performed angular intensity and spectra measurements. C.C. performed ray-tracing simulations. S.R.F. directed the research project. All authors contributed to data analysis and preparation of the manuscript.

Notes

The authors declare the following competing financial interest(s): S.R.F. has an equity interest in Universal Display Corp. This apparent conflict of interest is managed by the University of Michigan Office of Research.

REFERENCES

(1) Adachi, C.; Baldo, M. A.; Thompson, M. E.; Forrest, S. R. Nearly 100% Internal Phosphorescence Efficiency in an Organic Light-Emitting Device. *J. Appl. Phys.* **2001**, *90*, 5048−5051.

(2) Baldo, M. A.; O'Brien, D. F.; You, Y.; Shoustikov, A.; Sibley, S.; Thompson, M. E.; Forrest, S. R. Highly Efficient Phosphorescent Emission from Organic Electroluminescent Devices. *Nature* **1998**, *395* (6698), 151−154.

(3) Lamansky, S.; Djurovich, P.; Murphy, D.; Abdel-Razzaq, F.; Lee, H.-E.; Adachi, C.; Burrows, P. E.; Forrest, S. R.; Thompson, M. E. Highly Phosphorescent Bis-Cyclometalated Iridium Complexes: Synthesis, Photophysical Characterization, and Use in Organic Light Emitting Diodes. *J. Am. Chem. Soc.* **2001**, *123* (18), 4304−4312.

(4) Walzer, K.; Maennig, B.; Pfeiffer, M.; Leo, K. Highly Efficient Organic Devices Based on Electrically Doped Transport Layers. *Chem. Rev.* **2007**, *107* (4), 1233−1271.

(5) Brütting, W.; Frischeisen, J.; Schmidt, T. D.; Scholz, B. J.; Mayr, C. Device Efficiency of Organic Light-Emitting Diodes: Progress by

Improved Light Outcoupling. *Phys. Status Solidi A* **2013**, *210* (1), 44−65.

(6) Gather, M. C.; Reineke, S. Recent Advances in Light Outcoupling from White Organic Light-Emitting Diodes. *J. Photonics Energy* **2015**, *5* (1), 57607.

(7) Sun, Y.; Forrest, S. R. Organic Light Emitting Devices with Enhanced Outcoupling via Microlenses Fabricated by Imprint Lithography. *J. Appl. Phys.* **2006**, *100* (7), 07310610.1063/1.2356904.

(8) Koh, T.-W.; Spechler, J. A.; Lee, K. M.; Arnold, C. B.; Rand, B. P. Enhanced Outcoupling in Organic Light-Emitting Diodes via a High-Index Contrast Scattering Layer. *ACS Photonics* **2015**, *2* (9), 1366−1372.

(9) Jurow, M. J.; Mayr, C.; Schmidt, T. D.; Lampe, T.; Djurovich, P. I.; Brutting, W.; Thompson, M. E. Understanding and Predicting the Orientation of Heteroleptic Phosphors in Organic Light-Emitting Materials. *Nat. Mater.* **2016**, *15* (1), 85−91.

(10) Moon, C.-K.; Kim, K.-H.; Kim, J.-J. Unraveling the Orientation of Phosphors Doped in Organic Semiconducting Layers. *Nat. Commun.* **2017**, *8* (1), 791.

(11) B, W.; G, H.; Qiu, J.; P, P.; T, G.; M, H.; Wang, S.; W, L.; H, L. Unlocking the Full Potential of Organic Light-Emitting Diodes on Flexible Plastic. *Nat. Photonics* **2011**, *5* (12), 753−757.

(12) Schwab, T.; Schubert, S.; Hofmann, S.; Fröbel, M.; Fuchs, C.; Thomschke, M.; Müller-Meskamp, L.; Leo, K.; Gather, M. C. Highly Efficient Color Stable Inverted White Top-Emitting OLEDs with Ultra-Thin Wetting Layer Top Electrodes. *Adv. Opt. Mater.* **2013**, *1* (10), 707−713.

(13) Bocksrocker, T.; Preinfalk, J. B.; Asche-Tauscher, J.; Pargner, A.; Eschenbaum, C.; Maier-Flaig, F.; Lemme, U. White Organic Light Emitting Diodes with Enhanced Internal and External Outcoupling for Ultra-Efficient Light Extraction and Lambertian Emission. *Opt. Express* **2012**, *20* (S6), A932−A940.

(14) Reineke, S.; Lindner, F.; Schwartz, G.; Seidler, N.; Walzer, K.; Lüssem, B.; Leo, K. White Organic Light-Emitting Diodes with Fluorescent Tube Efficiency. *MRS Online Proc. Libr.* **2009**, *1212*10.1557/PROC-1212-S02-06.

(15) Chang, H.-W.; Lee, J.; Hofmann, S.; Hyun Kim, Y.; Müller-Meskamp, L.; Lüssem, B.; Wu, C.-C.; Leo, K.; Gather, M. C. Nano-Particle Based Scattering Layers for Optical Efficiency Enhancement of Organic Light-Emitting Diodes and Organic Solar Cells. *J. Appl. Phys.* **2013**, *113* (20), 20450210.1063/1.4807000.

(16) Kim, J.-B.; Lee, J.-H.; Moon, C.-K.; Kim, S.-Y.; Kim, J.-J. Highly Enhanced Light Extraction from Surface Plasmonic Loss Minimized Organic Light-Emitting Diodes. *Adv. Mater.* **2013**, *25* (26), 3571−3577.

(17) Qu, Y.; Slootsky, M.; Forrest, S. R. Enhanced Light Extraction from Organic Light-Emitting Devices Using a Sub-Anode Grid. *Nat. Photonics* **2015**, *9* (11), 758−763.

(18) Qu, Y.; Coburn, C.; Fan, D.; Forrest, S. R. Elimination of Plasmon Losses and Enhanced Light Extraction of Top-Emitting Organic Light-Emitting Devices Using a Reflective Sub-Electrode Grid. *ACS Photonics* **2017**, *4*, 36310.1021/acsphotonics.6b00847.

(19) Lee, K. M.; Fardel, R.; Zhao, L.; Arnold, C. B.; Rand, B. P. Enhanced Outcoupling in Flexible Organic Light-Emitting Diodes on Scattering Polyimide Substrates. *Org. Electron.* **2017**, *51*, 471−476.

(20) Sun, Y.; Forrest, S. R. Enhanced Light out-Coupling of Organic Light-Emitting Devices Using Embedded Low-Index Grids. *Nat. Photonics* **2008**, *2* (8), 483−487.

(21) Jeon, S.; Lee, S.; Han, K.-H.; Shin, H.; Kim, K.-H.; Jeong, J.-H.; Kim, J.-J. High-Quality White OLEDs with Comparable Efficiencies to LEDs. *Adv. Opt. Mater.* **2018**, *6*, 170134910.1002/adom.201701349.

(22) Komoda, T.; Yamae, K.; Kittichungchit, V.; Tsuji, H.; Ide, N. 45.2: Invited Paper: Extremely High Performance White OLEDs for Lighting. *Dig. Tech. Pap. - Soc. Inf. Disp. Int. Symp.* **2012**, *43* (1), 610−613.

(23) Ou, Q.-D.; Zhou, L.; Li, Y.-Q.; Shen, S.; Chen, J.-D.; Li, C.; Wang, Q.-K.; Lee, S.-T.; Tang, J.-X. Extremely Efficient White Organic Light-Emitting Diodes for General Lighting. *Adv. Funct. Mater.* **2014**, *24* (46), 7249−7256.

(24) Kato, K.; Iwasaki, T.; Tsujimura, T. Over 130 lm/W All-Phosphorescent White OLEDs for Next-Generation Lighting. *J. Photopolym. Sci. Technol.* **2015**, *28* (3), 335−340.

(25) Chang, Y.-L.; Song, Y.; Wang, Z.; Helander, M. G.; Qiu, J.; Chai, L.; Liu, Z.; Scholes, G. D.; Lu, Z. Highly Efficient Warm White Organic Light-Emitting Diodes by Triplet Exciton Conversion. *Adv. Funct. Mater.* **2013**, *23* (6), 705−712.

(26) Callens, M. K.; Yokoyama, D.; Neyts, K. Anisotropic Materials in OLEDs for High Outcoupling Efficiency. *Opt. Express* **2015**, *23* (16), 21128−21148.

(27) Tsai, C.-H.; Tien, K.-C.; Chen, M.-C.; Chang, K.-M.; Lin, M.-S.; Cheng, H.-C.; Lin, Y.-H.; Chang, H.-W.; Lin, H.-W.; Lin, C.-L.; Wu, C.-C. Characterizing Coherence Lengths of Organic Light-Emitting Devices Using Newton's Rings Apparatus. *Org. Electron.* **2010**, *11* (3), 439−444.

(28) Forrest, S. R.; Bradley, D. D. C.; Thompson, M. E. Measuring the Efficiency of Organic Light-Emitting Devices. *Adv. Mater.* **2003**, *15* (13), 1043−1048.